SeaWinds validation with research vessels

Mark A. Bourassa, David M. Legler,[1] James J. O'Brien, and Shawn R. Smith
Center for Ocean-Atmospheric Prediction Studies, Florida State University, Tallahassee, Florida, USA

Received 14 June 2001; revised 5 December 2001; accepted 17 December 2001; published 6 February 2003.

[1] The accuracy of the SeaWinds scatterometer's vector winds is assessed through comparison with research vessel observations. Factors that contribute to uncertainty in scatterometer winds are isolated and examined as functions of wind speed. For SeaWinds on QuikSCAT, ambiguity selection is found to be near perfect for surface wind speed (w) > 8 m s^{-1}; however, ambiguity selection errors cause directional uncertainty to exceed 20° for $w < \sim$5 m s^{-1}. These average uncertainties for wind speed and direction are found to be 0.45 m s^{-1} and 5° for the QSCAT-1 model function and 0.3 m s^{-1} and 3° for the Ku-2000 model function. The QuikSCAT winds are examined as vectors through two new approaches. The first is a method for determining vector correlations that considers uncertainty in the comparison data set. The second approach is a wind speed-dependent model for the uncertainty in the magnitude of vector errors. For the QSCAT-1 (Ku-2000) model function this approach shows ambiguity selection dominates uncertainty for 2.5 < w < 5.5 m s^{-1} (0.6 < w < 5.5 m s^{-1}), uncertainty in wind speed dominates for w < 2.5 m s^{-1} and 5.5 < w < 7.5 m s^{-1} (w < 0.6 m s^{-1} and 5.5 < w < 18 m s^{-1}), and uncertainty in wind direction (for correctly selected ambiguities) dominates for w > 7.5 m s^{-1} (w > 18 m s^{-1}). This approach also shows that spatial variability in the wind direction, related to inexact spatial co-location, is likely to dominate rms differences between scatterometer wind vectors and in situ comparison measurements for w > 4.5 m s^{-1}. The techniques used herein are applicable to any validation effort with uncertainty in the comparison data set or with inexact co-location. *INDEX TERMS:* 3339 Meteorology and Atmospheric Dynamics: Ocean/atmosphere interactions (0312, 4504); 4275 Oceanography: General: Remote sensing and electromagnetic processes (0689); 4504 Oceanography: Physical: Air/sea interactions (0312); 4594 Oceanography: Physical: Instruments and techniques; 9805 General or Miscellaneous: Instruments useful in three or more fields; *KEYWORDS:* remote sensing, SeaWinds, validation, ocean, winds

Citation: Bourassa, M. A., D. M. Legler, J. J. O'Brien, and S. R. Smith, SeaWinds validation with research vessels, *J. Geophys. Res.*, *108*(C2), 3019, doi:10.1029/2001JC001028, 2003.

1. Introduction

[2] Ocean vector winds, critical for determining the dynamical forcing of the ocean, are sensitive indicators of the surface manifestation of over-ocean atmospheric phenomena. Applications of NASA scatterometer (NSCAT) observations demonstrated the remarkable uses for plentiful high quality wind vector observations: gap flow [*Bourassa et al.*, 1999b; *Chelton et al.*, 2000a, 2000b], pressure fields [*Foster et al.*, 1999; *Zierden et al.*, 2000], forcing ocean models [*Milliff et al.*, 1999a; *Verschell et al.*, 1999], and studies in regions with sparse in situ coverage [*Bourassa et al.*, 1999b; *Milliff et al.*, 1999b; *Chelton et al.*, 2000a, 2000b]. SeaWinds on QuikSCAT was commissioned to fill the untimely gap in wide-swath ocean vector wind observations due to the catastrophic failure of the Advanced Earth Observing Satellite (ADEOS-1), which carried NSCAT. Another SeaWinds instrument will be operational aboard ADEOS-2 in 2003.

[3] The accuracy of vector winds from the SeaWinds scatterometer on the QuikSCAT satellite is assessed through comparison with observations from research vessels. Differences in sampling characteristics are examined to select an averaging scheme for the ship data that minimizes the differences between the two sets of observations. Sources of difference between satellite and in situ observations are separated into six independent components: rain contamination, ambiguity selection, scatterometer wind direction errors for correctly selected ambiguities, scatterometer wind speed errors, errors in the surface comparison observations, and spatial variability due to inexact co-location. Rain-related errors are not directly considered in this study because they are a function of wind speed and rain rate [*Weissman et al.*, 2000]; hence rain-related errors vary on an event to event bases, and they cannot be treated as random errors. Consideration of the last two components is essential to an accurate estimate of uncertainty in all situations were there is no absolute standard of truth and when the comparison data sets cannot be exactly co-located. Use of similar

[1] Now at U.S. CLIVAR Office, Washington, D. C., USA.

0148-0227/03/2001JC001028$09.00

Table 1. Vessels Used in SeaWinds on QuikSCAT Validation and the Range of U_{10EN} and Dimensionless Atmospheric Stability (z/L; Where z = 10 m, and L is the Obhukov Scale Length) for Co-located Observations

Ship	Location	Time	Range of U_{10EN}, m s^{-1}	Range of Atmospheric Stabilities (z/L)
R/V *Atlantis*	Gulf of Alaska	July and Aug. 1999	4–10	−0.44 to 0.01
RSV *Aurora Australis*	Southern Ocean	July to Sept. 1999	4.5	−0.04
R/V *Knorr*	North and equatorial Atlantic	Jan.–June 2000	1–16	−8.1 to −0.01
R/V *Melville*	tropical Pacific	July–Nov. 1999	2–11	−9.2 to −4.5
R/V *Meteor*	North Atlantic	July 1999 to Aug. 2000	1–16	−3.5 to −4.3
R/V *Oceanus*	North Atlantic	July–Dec. 1999 and April 2000	2–13	−2.7 to −0.37
R/V *Polarstern*	North Atlantic	July 1999 to June 2000	1–19	−8.3 to 5.3
R/V *Ronald Brown*	tropical Pacific	July–Sept. 1999	1–7	−6.5 to −0.09

techniques in the validation of other sensors should result in much better estimates of uncertainty.

[4] The accuracy of QuikSCAT wind vectors is examined through two new approaches. The first is a method for determining vector correlations that explicitly considers errors and uncertainty in the comparison measurements. Correlation analysis typically implicitly considers one set of observations as errorless (truth) and examines variance relative to this truth (i.e., differences are measured perpendicular to the axis of the comparison data). Such correlation techniques underestimate the fraction of variance explained by a linear relation between the two data sets. This problem can be a serious for instruments with accuracy that is similar to or better than that of comparison measurements.

[5] The second approach to vector analysis is a wind speed-dependent model of vector uncertainty. This approach is valid only for wind speeds greater than a threshold that is a function of the uncertainties in both wind speed observations [*Freilich*, 1997]. Below this threshold (several times the larger uncertainty), random component errors are a better model of observational uncertainties. However, we will show that random component errors are inconsistent with results for 10 m wind speeds $w_{10} > 7$ m s^{-1}. In our model of vector uncertainty, errors are modeled as a non-isotropic Gaussian distribution about the head of the wind vector. The uncertainty in the magnitude of vector errors (i.e., the spread about the head of the wind vector) is modeled in terms of uncertainties in ambiguity selection errors, wind direction uncertainty for correctly selected ambiguities, and wind speed uncertainty. The relative importance of these terms is shown and compared to variability resulting from inexact spatial co-location with the surface measurements. The results demonstrate the high quality of SeaWinds vector winds.

2. Data

[6] The remotely sensed winds will be validated through comparison with in situ wind measurements. The remotely sensed winds were from the SeaWinds scatterometer on the QuikSCAT satellite, using the QSCAT-1 and Ku-2000 geohysical model functions (GMFs). The QSCAT-1 scatterometer data were obtained from the NASA Physical Oceanography Distributed Active Archive Center (PO.DAAC) at the Jet Propulsion Laboratory/California Institute of Technology, and the Ku-2000 scatterometer data was provided by Frank Wentz and Deborah Smith at Remote Sensing Systems. The winds from both model functions were considered in this study because both are likely to be used by the community. Knowledge of the relative strengths and weaknesses will be valuable to almost all users, and should help the developers of these data sets improve their products. In situ observations were gathered from automated weather systems on research vessels. The ship observations are available through the WOCE Data Archive Center (DAC) for surface meteorology at Florida State University. The ship observations represent many ocean and atmospheric conditions (Table 1); consequently, taken over the whole comparison set, there is unlikely to be a bias in these findings due to location (nor is there indication of such biases), a specific sea state, or atmospheric stability. There were 505 ship and SeaWinds co-locations that meet all our quality control constraints. The observed wind speeds ranged from 2 to 20 m s^{-1}.

2.1. Scatterometer Winds

[7] Scatterometers are unique among satellite remote sensors in their ability to determine surface wind speed and direction. Microwaves are scattered by short water waves (capillary and ultragravity waves), which respond quickly to changes in winds. The backscatter cross section (the fraction of transmitted energy that returns to the satellite) is a function of wind speed and wind direction relative to the orientation of the scatterometer. Scatterometers operate by acquiring multiple spatially and temporally co-located measurements of backscattered power from different viewing geometries. The known relationship between cross section, wind velocity, and viewing geometry is then used to estimate wind speed and direction [*Naderi et al.*, 1991].

[8] Ku band scatterometers (NSCAT and SeaWinds) are calibrated to "equivalent neutral wind speeds" [*Liu and Tang*, 1996; *Verschell et al.*, 1999; *Mears et al.*, 2001] at a height of 10 m above the local mean water surface. Equivalent neutral wind speeds differ from wind speeds that would be measured by anemometers after adjustment to a height of 10 m. These differences are a function of atmospheric stratification and are usually <0.5 m s^{-1} (hereafter equivalent neutral winds will be referred to as winds). For this validation, a boundary layer model [*Bourassa et al.*, 1999a] is used to adjust the research vessel winds to 10 m equivalent neutral winds.

[9] The relationship between backscatter cross section and relative wind direction, at fixed wind speed and incidence angle, is sinusoidal [*Naderi et al.*, 1991; *Wentz and Smith*, 1999]. Consequently, the measure of misfit for the satellite relative wind direction is sinusoidal in wind direction, which typically results in 1–4 local minima (see *Naderi et al.* [1991] for a detailed discussion). Ideally, the best fit corresponds to the correct direction. Noise in the observed backscatter cross sections can alter the depend-

ence of misfit on relative wind direction and thereby cause incorrect directions (also known as aliases) to be chosen. For previous scatterometers (with fixed beam antennas), the second best fit is typically in the opposite direction, and the third and fourth minima are typically in directions roughly perpendicular to the wind direction. For NSCAT, the results of a median filter were compared to each of the ambiguous directions to determine which ambiguity was selected. This process requires an initial guess at the correct ambiguity: the ambiguity (of the two most likely ambiguities) with the direction that was the closest match to the direction from the National Centers for Environmental Prediction (NCEP) 2.5° analysis [*Shaffer et al.*, 1991]. The use of an analysis with coarse resolution compared to the scatterometer observations can result in erroneous ambiguity selection. However, this approach leads to more accurate ambiguity selection than the use of the median filter alone [*Wentz and Smith*, 1999].

[10] NSCAT had many similarities to SeaWinds in both design and processing of the backscatter to winds. Comparisons of NSCAT winds to in situ observations include data from buoys [*Graber et al.*, 1997; *Caruso et al.*, 1999; *Atlas et al.*, 1999; *Freilich and Dunbar*, 1999], volunteer observing ships [*Atlas et al.*, 1999], and research vessels [*Bourassa et al.*, 1997]. These studies investigated the accuracy of wind speed, wind direction (usually for correctly selected ambiguities), and vector winds [*Freilich and Dunbar*, 1999], as well as the likelihood of correct ambiguity selection. They determined the RMS difference between NSCAT and in situ winds, which provides an upper limit on uncertainty in NSCAT winds: substantial fractions of the differences are likely due to uncertainty in the comparison measurements and space-time differences in the co-located observations. An additional cause of differences is geophysical: ship and buoy winds are usually Earth relative, whereas scatterometer winds are surface (current) relative. These errors are significant in areas of strong currents [*Cornillon and Park*, 2001; *Kelley et al.*, 2001]. NSCAT RMS differences were $\sim$1.2 m s^{-1} [*Freilich and Dunbar*, 1999; *Freilich and Vanhoff*, 2002], 13° for correctly chosen ambiguities (and $w > 4$ m s^{-1}); [*Bourassa et al.*, 1997], with 90% accuracy in ambiguity selection [*Gonzales and Long*, 1999]. Most of the errors in ambiguity selection occurred for $w < 4$ m s^{-1}, with a much smaller fraction for $4 < w < 6$ m s^{-1}, and a nearly negligible fraction for $w > 8$ m s^{-1} [*Bourassa et al.*, 1997; *Freilich and Vanhoff*, 2002].

[11] The SeaWinds scatterometer uses a new radar design with two conically rotating pencil beams. These beams have incidence angles of 46.25° and 54°. The inner beam has a radius of 707 km, and the outer beam has a radius of 900 km. Individual footprints are binned into 25 × 25 km cells, with up to 76 cells across the satellite swath (Figure 1). This geometry is expected to result in relatively accurate observations between $\sim$200 and 700 km from nadir, with the greatest uncertainties farthest away and closest to nadir. Typical 25 × 25 km vector wind cells contain the centers of 10–25 25 × 35 km oval radar footprints. All footprints with centers within the cell are applied to determining the winds, which results in radar returns being gathered from an area of $\sim$50 × 60 km^2. We will show that the scatterometer's sampling characteristics are better matched to winds on substantially smaller spatial scales.

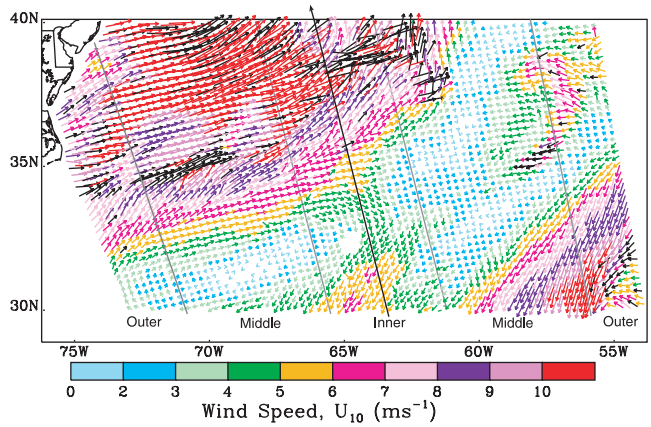

Figure 1. Example of a SeaWinds observation swath (QSCAT-1 GMF and MUDH rain flag) for 09:48 to 09:51 UTC on September 20, 2000. Only selected ambiguities are shown, and there is no smoothing. Vectors identified as rain contaminated are black. Arrow lengths are proportional to wind speed. Accuracy is dependent on across-swath position. We divide the swath into three categories that are symmetric about nadir (solid line): inner swath (<200 km from nadir; cells 31–46), middle swath (cells 9–30 and 47–68), and outer swath (>700 km from nadir; cells 1–8 and 69–76). The borders of these regions are shown by the shaded lines.

[12] SeaWinds' new beam geometry results in much more diverse solution geometries. Solutions from two ambiguity removal techniques are available in the JPL's QuikSCAT dataset. The standard product uses the ambiguity selection technique applied to NSCAT. The second product, Direction Interval Retrieval THreshold (DIRTH) [*Huddleston and Stiles*, 2000], attempts to better account for the more complex SeaWinds solution geometry. DIRTH was developed to reduce the relatively large uncertainty near nadir and at the edges of the swath. The DIRTH vector field is smoother than the standard product, thereby reducing the correlation to point observations (which include small-scale variability). Consequently, this analysis will be confined to the standard product.

[13] Rain can have a substantial influence on SeaWinds observations. Rain influences radar returns through three processes: backscatter from the rain, attenuation of the signal passing through the rain [*Moore et al.*, 1999], and modification of the surface shape by raindrop impacts [*Bliven et al.*, 1993; *Sobieski and Bliven*, 1995; *Sobieski et al.*, 1999]. The influence of these considerations on the accuracy of winds is a function of scatterometer design. Rain has a greater influence at large incidence angles (the beam interacts with more rain) and for Ku band (NSCAT and SeaWinds) rather than C band (ERS-1/2). Modeling these problems is a concern of ongoing research; however, a theoretical basis for modeling the errors now exists [*Weissman et al.*, 2000] and should help develop retrieval algorithms that better account for rain.

[14] Several rain flags are being developed based on scatterometer observations, coincident radiometer rain rates (from other satellites) or a combination of these data. Four such flags are examined herein. The normalized objective Function (ENOF) flag [*Mears et al.*, 2000] is based on

Table 2. Biases (Scatterometer Minus Ship) in Speed (m s^{-1}; for All Selected Ambiguities) and Direction (Degrees, in Meteorological Direction Convention; for Correctly Selected Ambiguities) for Selected Research Vessels

Biases	*Atlantis*	*Melville*	*Meteor*	*Oceanus*	*Polarstern*	All Ships
QSCAT-1 speed	0.2 ± 0.2	0.18 ± 0.1	0.06 ± 0.1	0.4 ± 0.3	0.0 ± 0.06	0.06 ± 0.05
Ku-2000 speed	0.7 ± 0.07	−0.4 ± 0.3	−0.18 ± 0.02	−0.12 ± 0.1	−0.14 ± 0.02	−0.01 ± 0.01
QSCAT-1 direct.	5 ± 3	1.8 ± 1	−4.6 ± 1	−3.4 ± 3	−2.3 ± 1	−1.6 ± 0.7
Ku-2000 direction	10 ± 2	...	−0.7 ± 0.2	−4.4 ± 2	−4.6 ± 0.2	−1.99 ± 0.09

Uncertainties correspond to one standard deviation.

variability in the normalized radar cross sections within a wind cell, calculated relative to the value consistent with the selected wind vector. The multidimensional histogram (MUDH) flag [*Huddleston and Stiles*, 2000] is based on a probability space determined from four of six parameters that are sensitive to rain. Both the ENOF and MUDH rain flags are in JPL's data set. The SeaWinds data set available from Remote Sensing Systems (RSS) contains four rain flags, well designed for combination into a single rain flag that can be tailored to an application. In this case, the following flags and criteria were used to produce a single flag for rain: (1) Ku-2000 ''quality of retrieval'' flag (iclass) = 0 (no retrieval), or (2) Ku-2000 scatterometer-based flag (rflag_scat) = 1, or (3) Ku-2000 fit to GMF flag (sos_all) > 1.9, or (4) Ku-2000 radiometer-based (rad_rain) flag > 0.15 and difference in temporal co-location <30 min. These four flags are combined as suggested by RSS, with the exception of condition (1), which is more generous than suggested, and is similar to the flags in JPL's product. We examine this single (multisource) rain flag as well as the RSS rain flag based solely on co-locations with radiometers on other platforms (SSM/I and TMI). The key shortcoming of a rain flag based solely on off-board devises is the large fraction of wind observations that were not co-located with rain observations. Only 50% of QuikSCAT and ship co-locations were co-located (3 hours and 50 km) with SSMI observations; and the co-location in time must be much closer than 3 hours due to the rapid variability in rain rates.

2.2. Research Vessel Winds

[15] Wind direction measurements from research vessels have proven to be the most consistently accurate source of in situ wind direction [*Bourassa et al.*, 1997]. True winds (i.e., speeds relative to the fixed Earth and directions relative to true north) that are correctly calculated from ship-relative observations [*Smith et al.*, 1999], do not suffer from the intermittent quality of buoy winds found by *Freilich and Dunbar* [1999] or the large uncertainties in VOS observations [*Pierson*, 1990; *Kent et al.*, 1998]. Preliminary comparisons between VOS and NSCAT winds found that the RMS differences in wind speeds that were roughly three times as large as the differences with quality-controlled research vessel winds (V. Zlotnicki and R. Atlas, personal communications, 1997). Research vessel data have errors due to insufficient maintenance and erroneous calculation of true (Earth relative) winds [*Smith et al.*, 1999]. Automated quality control and limited visual inspection [*Smith et al.*, 1996] identified and flagged serious errors. The most common problem, incorrect calculation of true winds from ship-relative winds, was solved by recalculation of the true winds [*Smith et al.*, 1999]. Another advantage of ship observations over buoy observations is that the observation height is above the regime where wave motions modify the log wind profile [*Large et al.*, 1995], which is not the case for buoys in heavy seas. In very stable air, ship (and occasionally buoy) anemometers can be above the height of the log profile layer; these occurrences are rare and usually restricted to vessels with very high masts (S. Goodrick, personal communication, 1998). Research ships record the temperature and humidity information needed as input to a boundary layer model [*Bourassa et al.*, 1999a] to adjust the anemometer measurements to a height of 10 m (the height to which the scatterometer winds are calibrated) equivalent neutral winds. Errors in height adjustment are small compared to other shortcomings of ship observations.

[16] The major shortcoming of ship observations is the impact of flow distortion on wind directions and speeds [*Yelland et al.*, 1998; *Kent et al.*, 1998; *Taylor et al.*, 1999]. Flow distortion errors greatly exceed the uncertainty in mean winds (e.g., averaged over 5 min) sampled in 60 s intervals. This problem is reduced by eliminating winds from ship-relative angles for which the winds would have passed through or near the superstructure, and through quality control of the observations. The worst cases of flow distortion are eliminated through our constraints on ship-relative wind directions (±30° about the aft for bow mounted sensors, and within ±60° of the port or starboard for side mounted sensors). Much of the wind observation record from the R/V *Ronald Brown* were discarded during our quality control of the ship data (prior to comparison with the scatterometer); most cruises during this time period suffered from severe flow distortion (C. Fairall, personal communication, 2000). Nevertheless, flow distortion causes biases that vary from ship to ship, depend on anemometer location, and vary cruise to cruise due to repositioning of equipment [*Taylor et al.*, 1999]. These biases are dependent on ship-relative wind direction, and appear as random noise in the set of co-located wind vectors; however, observations from a single leg of a cruise could have directional biases due to little variability in ship-relative wind direction. The bias in QuikSCAT speed (relative the ships used in this study; Table 2) ranges from 0.0 to 0.4 m s^{-1} for the QSCAT-1 GMF (−0.4 to + 0.7 m s^{-1} for the Ku-2000 GMF), with most speed biases being within ±0.2 m s^{-1}. One potential application of high quality scatterometer data is the estimation of biases due to flow distortion. In less than a year of open-ocean operations, there would be sufficient observations (an average of two per day for QuikSCAT) to examine the problem as a function of wind speed and ship-relative wind direction.

[17] Another minor shortcoming of ship data is that 1-min sampling intervals are insufficient to remove averaging errors associated with ship acceleration. These errors are

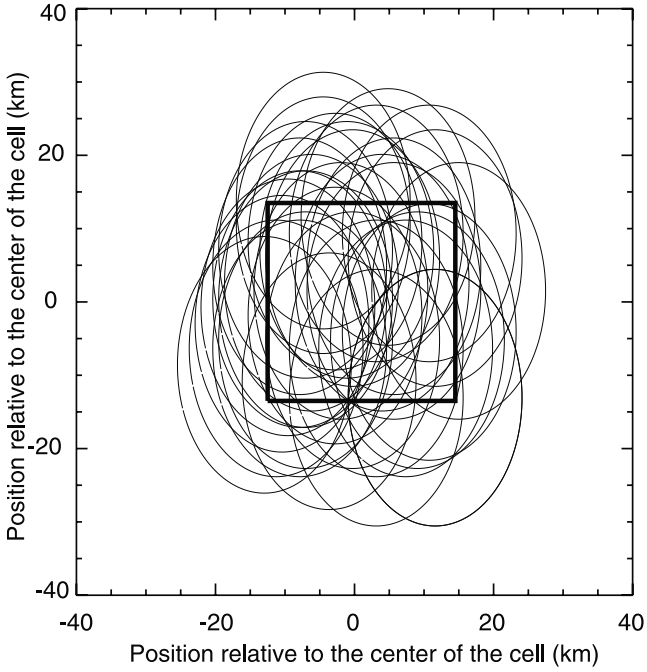

Figure 2. Example of backscatter footprints within a SeaWinds vector wind cell. Each oval represents one backscatter observation.

due to averaging nonlinear equations where the ship's speed and/or direction are changing. For research vessels, the errors in speed during the first few minutes of acceleration are typically 1–2 m s^{-1} [*Smith et al.*, 1999]. These errors are sufficiently large and frequent enough to have caused a statistically significant increase in RMS differences between NSCAT and research vessels wind speeds [*Smith et al.*, 1999]. In 1999, the wind calculation on the *Polarstern* was changed to process true winds every 5 s and average them every minute. The acceleration-related (averaging) errors are not evident in the winds recorded by this system. Ship winds associated with excessive ship acceleration are eliminated through a criterion developed by *Smith et al.* [1999]: the magnitude of the sum of variances in the component ship's velocities must be less than 1.0 m^2 s^{-2}.

2.3. Co-Locations and Matching Sampling Characteristics

[18] The uncertainty in the comparison measurements at the location of the satellite observation is reduced by restricting this analysis to a set of coincident satellite and high quality research vessel observations. The differences in the central (mean) observation times are less than 20 min (usually <30 s), and the largest differences in location are <12.5 km (half the scatterometer cell width). The co-located winds are also quality controlled to remove gross errors in wind speeds (presumably related to unflagged rain) following the criteria of *Freilich and Dunbar* [1999]. All scatterometer data flagged as rain contaminated are discarded, as are those with missing rain flags. The estimated uncertainties are dependent on the choices of co-location criteria and rain flag. There are several SeaWinds-based rain flags in use, as well as a flag based on instruments (SSM/I and TMI) aboard other satellites. Each of these rain flags will be considered in various aspects of this evaluation of SeaWinds accuracy.

[19] The high temporal resolution of the research vessel observations provides the opportunity to investigate the optimal averaging scheme to match a series of point observations with the scatterometer observations. There are typically 8–20 radar cross-section observations (footprints) that are combined in each 25 × 25 km scatterometer wind cell (Figure 2). The distribution of footprints within the cell is nonuniform, with the average observation density greatest at the center of the cell and falling by a factor of four at the corners of the cell. The time over which the radar cross sections are gathered is also a function of the position across the satellite track. The averaging period is near instantaneous at the swath edge and increases to ~4 min near nadir. These differences suggest that the optimal averaging period for ship data might be a function of cross-track position, which is confirmed in our results (Figure 3). It is also apparent (Figure 3) that the choice of sampling volume for the ship data can influence the comparison. A preliminary examination showed that averaging over fixed times (examined over a wide range of time intervals) had little influence on RMS difference or vector correlations for most wind speed ranges. For high wind speeds, short averaging times (several minutes) clearly resulted in smaller RMS differences; for low wind speeds much longer averaging times (30+ min) were superior. The change in optimum averaging time with wind speed results can be anticipated from Taylor's hypothesis [*Taylor*, 1938]. Therefore, we examined the influence of the ship's sampling "volume" (equivalent to a length scale for point observations) as estimated from the ship relative wind speeds. For most parts of the swath, there is a local or global minimum

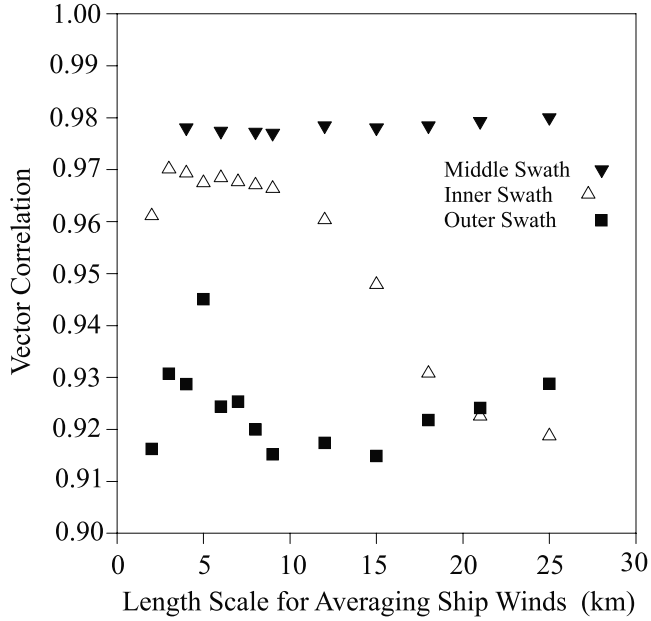

Figure 3. Vector correlation (section 5.2) as a function of position across the swath and lengthscale for the ship's sampling volume. The sampling volume is estimated from the ship-relative wind speeds. The spatial co-location criterion is 8 km.

at a length scale at or near 5 km. This result is not directly indicative of the resolution of the scatterometer: it indicates a spatial-temporal scale where the balance between signal and noise in the research vessel observations result in the best matches the scatterometer winds. Averaging over this length scale resulted in slightly smaller (at least 10%) RMS differences compared to any fixed averaging time. The ship observations were averaged over a sampling volume of approximately 5 km for the remainder of this study.

3. Ambiguity Selection Accuracy

[20] The patterns of wind vector cell ambiguous solutions are more diverse for a SeaWinds instrument than a fixed beam instrument. For SeaWinds, the solution geometry is also a function of the distance from nadir (Figure 1). For parts of the swath covered by both beams but not too close to nadir (200–700 km from nadir, hereafter referred to as the middle swath), the patterns of ambiguities are similar to those found with NSCAT (assuming a similar GMF): there are usually large angles (>30°) between the ambiguities. However, for the outer swath (>700 km from nadir) and the inner swath (<200 km from nadir) pairs of ambiguities are more likely to be <30° apart. For such situations, difference between satellite and in situ measurements makes it difficult to determine which of the similar directions is correct. Pairs of SeaWinds ambiguities are more likely than NSCAT ambiguities to converge to a single solution, resulting in two ambiguous solutions rather than four. We examine only gross errors in ambiguity selection: all selected ambiguities within 45° of the surface measurements are considered to be correctly chosen.

[21] Ambiguity selection errors tend to occur in areas of low wind speed, areas with large change in wind direction between adjacent scatterometer cells (fronts and low pressure systems), and near rain. The fraction of correctly selected ambiguities is also a function of wind speed and across-swath location. The accuracy of SeaWinds ambiguity selection skill, averaged across the swath (Figure 4a) is compared to the skill in the 25 and 50 km resolution NSCAT products. QuikSCAT ambiguity selection skill is excellent for $w > 4$ m s^{-1} and is a great improvement over NSCAT for $w < 4$ m s^{-1}. Ambiguity selection skill is also a weak function of cross-swath position (Figure 4b): the most accurate QSCAT-1 ambiguity selection occurs away from nadir and away from the edges of the swath. This result is consistent with visual inspection of the SeaWinds swaths, which have greater cross-swath variability near nadir and near the swath edges. Ambiguity selection skill for the Ku-2000 GMF is similar in magnitude to QSCAT-1 skill; however, it has much less across-swath dependence. The main difference is in the inner swath, where Ku-2000 skill is superior to the QSCAT-1 skill.

[22] The limited geographic distribution of wind speeds sampled from the research vessels is not representative of the global distribution sampled by QuikSCAT; therefore, the fraction of correctly selected ambiguities based on ship observations (91.8% for QSCAT-1 and 93.0% for Ku-2000) will differ from the global average. A better estimate of this global percentage is determined by applying the observed wind speed dependency to the distribution of wind speed observed by QuikSCAT. This approach results in an estimate of global accuracy at 92.6% for the QSCAT-1 GMF, and 93.3% for the Ku-2000 GMF.

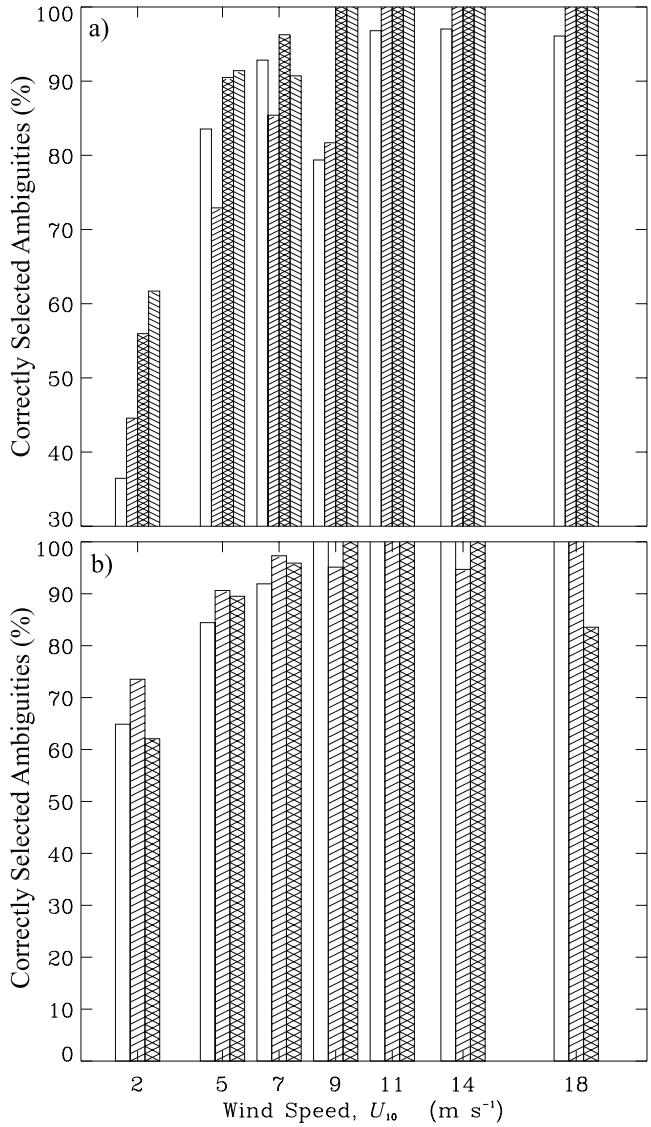

Figure 4. Ambiguity selection as a function of wind speed for (a) four ku-band scatterometer products (from left to right): the 25 and 50 km NSCAT products, the QSCAT-1 product, and the Ku-2000 product. NSCAT co-locations were within 25 km, whereas QuikSCAT co-locations are within 12.5 km. (b) QSCAT-1 ambiguity selection (applying the ENOF rain flag) is also a function of cross-swath position (from left to right): outer swath, middle swath, and inner swath.

4. Biases and RMS Differences

[23] Biases relative to individual ships are small (Table 2), indicating that regional biases are small. Trends in wind speed biases as a function of wind speed are also small (Figure 5). The apparent scatterometer overestimation for low wind speeds ($w < 3$ m s^{-1}) has been explained [*Freilich*, 1997; *Freilich and Dunbar*, 1999] as due to uncertainty in positive scalar quantities. The small bias (<1%) at high wind speeds could be due to flow distortion:

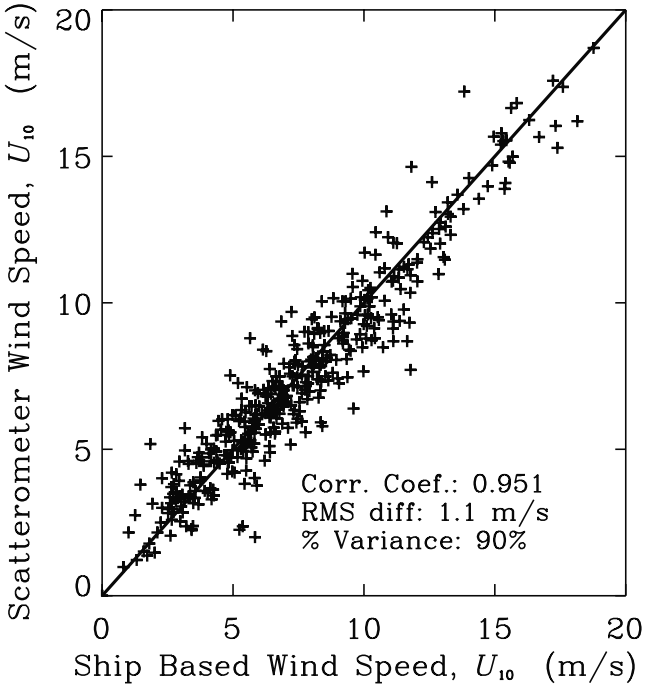

Figure 5. Scatterometer wind speed (QSCAT-1 model function; for correctly selected ambiguities) versus research vessel wind speed. Cross-swath dependence is weak for a 12.5 km co-location criterion. The line indicates a perfect fit.

the source of this bias cannot easily be verified [*Thiebaux*, 1990; *Taylor et al.*, 1999]. Flow distortion biases cannot be corrected for at this time, as the corrections are ship-dependent and costly to assess [*Yelland et al.*, 1998; *Taylor et al.*, 1999]. The magnitudes of the remaining wind speed biases are in the expected ranges for flow distortion problems. There is no strong evidence of a substantial systematic error in the QuikSCAT wind speeds.

[24] Biases in wind directions are slightly more difficult to assess due to the 0/360 breakpoint. This problem is solved modifying one set of directions:

$$\theta_R \rightarrow \theta_R + 360^\circ, \text{ when } \theta_R - \theta_I < -180^\circ \quad (1)$$

$$\theta_R \rightarrow \theta_R - 360^\circ, \text{ when } \theta_R - \theta_I > 180^\circ, \quad (2)$$

where θ_R is the remotely sensed direction, and θ_I is the in situ direction. The bias for the ensemble of all ships is <2° (scatterometer minus ship directions; meteorological direction convention).

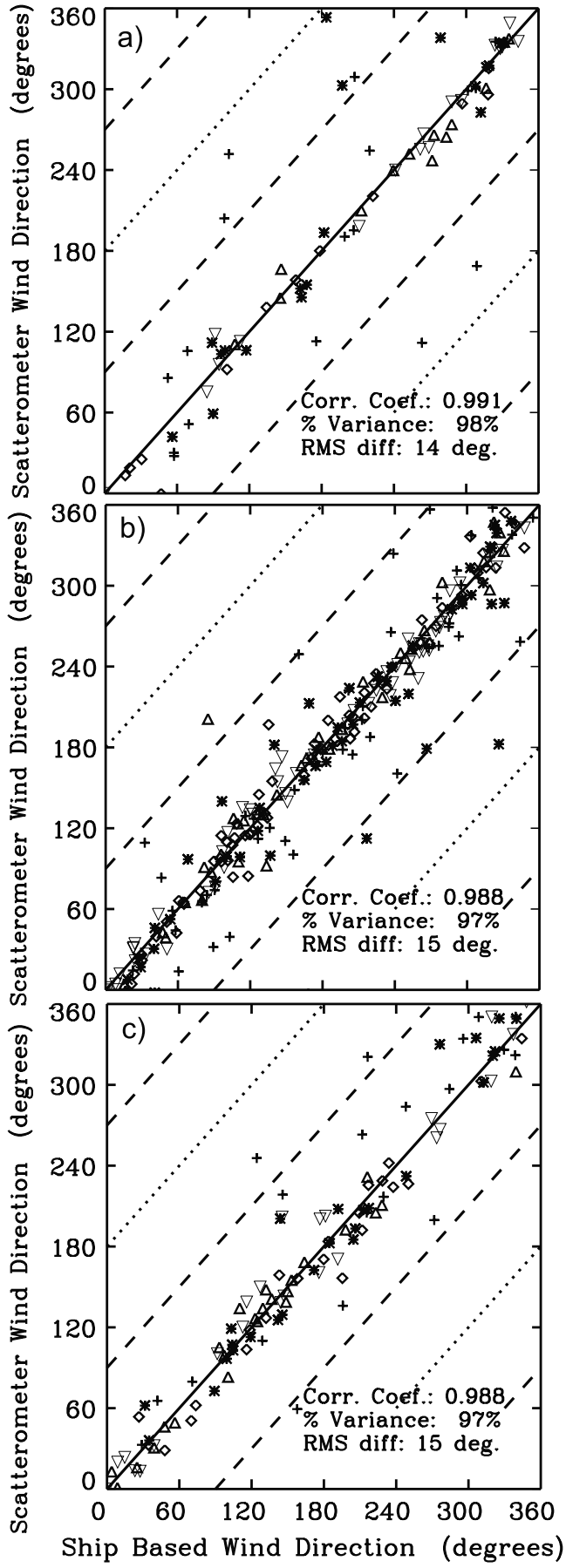

Figure 6. (opposite) Scatterometer wind (QSCAT-1 model function) direction versus research vessel wind direction for various region of the swath: (a) outer swath, (b) middle swath, and (c) near-nadir swath. The solid line indicates a perfect fit, the dashed lines are 90° errors, and the dotted lines are 180° errors. The symbols indicate wind speed ranges of (pluses) 0–4 m s^{-1}, (asterisks) 4–6 m s^{-1}, (diamonds) 6–8 m s^{-1}, (point-up triangles) 8–10 m s^{-1}, and (point-down triangles) 10–20 m s^{-1}. The statistics apply only to correctly selected ambiguities: those within 45° of the ideal line.

[25] Scatterplots of directions (Figure 6) are also extremely useful for visualizing random errors and errors in ambiguity selection. For previous scatterometers, ambiguity selection errors typically resulted in directional errors near 180° (most likely) or ±90°, and they were easily identified. With QuikSCAT's scanning geometry, only gross errors (herein differences >45°) are easily identified.

[26] Root mean square differences between satellite observations and surface measurements have been a common method for establishing an upper limit on the uncertainty of the satellite observations. These differences are shown (Table 3) for each GMF and rain flag, with all selected ambiguities, which provides an upper limit on uncertainty for the bulk of users who do not have the luxury of improving or testing the ambiguity selection. The second condition restricts the examination to correctly selected ambiguities (Table 3), which is more useful for identifying the independent contributions to the total uncertainty. The importance of successful ambiguity selection can be seen in Figures 7a and 7b and Table 3. The RMS differences for wind speed have little sensitivity to the restriction of correctly selected ambiguities: the RMS difference increasing $\sim$0.1 m s^{-1} when gross ambiguity errors are included in the comparison set. In contrast, direction-related differences are greatly influenced by the restriction of correctly selected ambiguities: for $w < 6$ m s^{-1}, RMS differences in wind direction (Figure 7b) increase by >100% when gross ambiguity selection errors are considered. Despite ambiguity selection that is quite effective relative to other scatterometers, errors in ambiguity selection make a major contribution to the uncertainty in QuikSCAT vector winds (particularly for $w < 6$ m s^{-1}).

[27] The choice of rain flag influences the misfit between ship and satellite winds (Table 3). Comparison of RMS differences for selected ambiguities shows that the radiometer rain flag is more effective than MUDH or ENOF for identification of rain contaminated observations. It also eliminates many rain-free observations where no radiometer observations were coincident with scatterometer observations. The rightmost columns in Table 3 show the QSCAT-1 and Ku-2000 RMS differences with the same radiometer rain flag. The Ku-2000 RMS differences are smaller, despite the larger biases (Table 2). The Ku-2000 improvements in directional accuracy (seen in the smaller uncertainties) are apparent in the relatively large improvements to accuracy of zonal and meridional wind components (Table 3). The Ku-2000 RMS differences for the product with all rain flags strongly suggest that rain-contaminated data without coincident radiometer observations are occasionally classified as rain free. The improved rain flags and directions in the Ku-2000 product result in a substantial reduction in RMS differences compared to the QSCAT-1 model function.

[28] For correctly selected ambiguities (defined herein as within 45° of the comparison data), the uncertainty has relatively little dependence on wind speed (Figures 7a

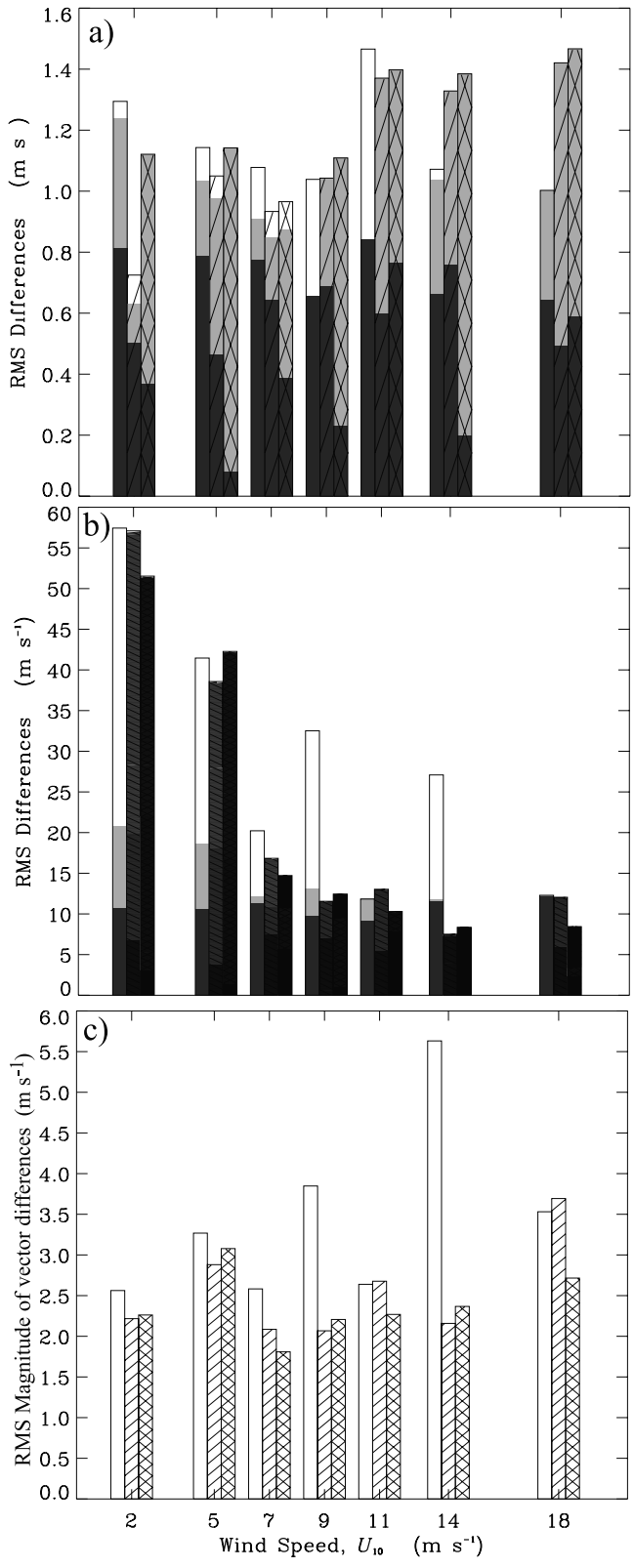

Figure 7. (opposite) Uncertainties in SeaWinds (a) wind speed and (b) direction as functions of ship wind speed for several QSCAT wind products: QSCAT-1 with MUDH rain flag (first column); Ku-2000 (second column); and Ku-2000 with radiometer rain flag (third column). The background shading indicates three difference measures of uncertainty: rms differences for all selected ambiguities (white), rms difference for correctly selected ambiguities (light shading), and PCA derived uncertainty (dark shading). Combinations of speed and direction errors are shown in (c) the rms average of vector wind difference magnitudes ($|\mathbf{u}_{scat} - \mathbf{u}_{ship}|$) as a function of wind speed.

Table 3. RMS Differences in Wind Speed (m s^{-1}), Wind Direction (Degrees), Zonal Wind Component (m s^{-1}), and the Meridional Wind Component (m s^{-1}) for Each of the GMFs and Various Rain Flags

	MUDH Rain Flag		ENOF Rain Flag		Radiom. Rain Flag	
QSCAT-1	Select Ambiguity	Correct Ambiguity	Select Ambiguity	Correct Ambiguity	Select Ambiguity	Correct Ambiguity
Wind speed	1.2	1.1	1.1	1.1	1.2	1.2
Wind direct.	...	15	...	15	...	15
Zonal wind	2.2	1.5	2.3	1.5	2.1	1.6
Meridional wind	2.7	1.6	2.5	1.5	2.2	1.4
Ku-2000	Ku 2000 Flags	Ku 2000 Flags			Radiom. Rain Flag	Radiom. Rain Flag
Wind speed	1.0	1.0			1.0	0.9
Wind direct.	...	14			...	14
Zonal wind	1.9	1.4			1.7	1.3
Meridional wind	1.8	1.4			1.7	1.3

Also shown is the importance of ambiguity selection. The criterion for spatial co-location is differences $\leq$12.5 km.

and 7b), and that dependency could be a consequence of minor (<45°) errors in ambiguity selection. The RMS magnitude of the wind vector differences (Figure 7c) has a stronger dependence on wind speed: there is a local peak for $4 > w > 6$ m s^{-1}, and for $w > 10$ m s^{-1} it increases with increasing wind speed (rapidly for the QSCAT-1 model function). This is a particularly useful diagnostic quantity because it can be used to distinguish between two models for SeaWinds uncertainty. For low wind speeds ($w < 4$ m s^{-1}), uncertainty has been very effectively modeled in terms of random vector component errors (σ_u, σ_v) [*Freilich*, 1997; *Freilich and Vanhoff*, 2002]. If the uncertainties in each component are equal ($\sigma_u = \sigma_v$), then the equation for the uncertainty in the magnitude of vector errors ($\sigma_{|\Delta \mathbf{w}|}$, where $\Delta \mathbf{w} = \mathbf{w}_{\text{scat}} - \mathbf{w}_{\text{ship}}$), described as a Gaussian distribution about the 'head' of the wind vector, with a standard deviation equal to $\sigma_{|\Delta \mathbf{w}|}$, is

$$\sigma^2_{|\Delta \mathbf{w}|} = 2\ \sigma^2_v, \tag{3}$$

which is independent of wind speed. Conceptually, this uncertainty should be the combination of two Gaussian distributions, one for uncertainty in the ship winds and one for uncertainty in scatterometer winds. The observed distributions (Figure 7c) are more consistent with constant uncertainties in wind speed (σ_w) and wind direction (σ_θ), for which the magnitude of vector uncertainty is

$$\begin{aligned}\sigma^2_{|\Delta \mathbf{w}|} &= \left(\frac{\partial(|\Delta \mathbf{w}|)}{\partial\, w}\right)^2 \sigma^2_w + \left(\frac{\partial(|\Delta \mathbf{w}|)}{\partial\, \theta}\right)^2 \sigma^2_\theta \\ &= \sigma^2_{w,\text{scat}} + \sigma^2_{w,\text{ship}} + w^2\left(\sigma^2_{\theta,\text{scat}} + \sigma^2_{\theta,\text{ship}}\right).\end{aligned} \tag{4}$$

This form of $\sigma_{|\Delta \mathbf{w}|}$ results in a nonisotropic error function, with different Gaussian distributions about w and ℓ axes (i.e., $\sigma_w \neq w\sigma_\theta$). For large wind speeds, the second term on the right hand side will dominate, and the uncertainty in wind vectors increases in proportion to the wind speed. Consequently, it is also apparent from (4) that, if vector component uncertainties are weakly dependent on wind speed (i.e., $\sigma^2_{|\Delta \mathbf{w}|}$ is approximately constant), then the directional uncertainty is proportional to w^{-1} for sufficiently large w. Such dependence is not found in the directional RMS differences, which further supports the need for a model of uncertainty that is appropriate for moderate and high wind speeds.

5. Improved Estimates of Quikscat Uncertainty

[29] Traditional statistical techniques, such as ordinary least squares fits and root mean square differences, presume that all uncertainty is related to one of the two sets of observations being compared. Incorrect estimates of uncertainty in the comparison measurements result in erroneous estimates of bias and gain of the observations as a function of comparison measurements [*Kent et al.*, 1998]: estimates of uncertainty in QuikSCAT winds should consider the uncertainty in comparison measurements [*Stoffelen*, 1998; *Freilich and Vanhoff*, 2002]. If the uncertainty in the comparison data set is known, then the uncertainty in the scatterometer can be determined through linear regression [*Stoffelen*, 1998]. Alternatively, if the uncertainty in the comparison data set is unknown, there are techniques that determine the uncertainty in both data sets [*Stoffelen*, 1998; *Freilich and Vanhoff*, 2002]. Uncertainty in the quality-controlled research vessel observations is small; however, it is unknown because it varies from ship to ship and cruise to cruise [*Smith et al.*, 1999]. Techniques that determine the uncertainty in both data sets require at least thousands of co-located observations from three sources. At this time, we have too few co-located observations to apply the techniques of *Stoffelen* [1998] or *Freilich and Vanhoff* [2002]. Furthermore, these methods do not distinguish between observational errors and geophysical differences (e.g., imperfect co-location and Earth relative versus surface relative winds). We will use an alternative approach to show that much of the uncertainty and RMS differences are due to the spatial separation between the research vessel and the center of the satellite footprint. The techniques of *Stoffelen* [1998] and *Freilich and Vanhoff* [2002] could be modified to consider spatial separation; however, currently they combine this source of uncertainty with error in the observations. Additional subtleties in the analysis of scalar winds have been identified [*Freilich*, 1997]. These complications involve low wind speeds and are greatly diminished by determining best fits using observations with $w > 3\ \sigma_w$ (where σ_w is the largest uncertainty in the two sets of speed observations).

Table 4. Variance Explained (%) Assuming the Uncertainty in the Scatterometer is Equal to the Uncertainty in the Research Vessels and That There are no Other Sources of Variability

	MUDH Rain Flag		ENOF Rain Flag		Radiom. Rain Flag	
QSCAT-1	Select Ambiguity	Correct Ambiguity	Select Ambiguity	Correct Ambiguity	Select Ambiguity	Correct Ambiguity
Wind speed	89	90	90	90	89	89
Wind direct.	...	97	...	97	...	97
Zonal wind	87	93	86	93	87	93
Meridional wind	80	93	83	93	85	93
Ku-2000	Ku-2000 Flags	Ku-2000 Flags			Radiom. Rain Flag	Radiom. Rain Flag
Wind speed	93	93			89	89
Wind direct.	–	97			...	97
Zonal wind	92	95			93	96
Meridional wind	90	94			88	93

The criterion for spatial co-location is differences $\leq$12.5 km.

[30] Principal component analysis (PCA) [*Preisendorfer and Mobley*, 1988; *Pearson*, 1901] assumes that there is equal uncertainty in each set of observations; therefore, it is ideal for the situation where the accuracy of the comparison data set is unknown and similar to the accuracy of the observations. For example, underestimation in the research vessels' uncertainty results in overestimation of QuikSCAT uncertainty. The assumption of similarity is valid if both uncertainties are small compared to the span of co-located observations. PCA can be used to estimate the uncertainty in terms of the standard deviation perpendicular to the axis of maximum variance.

5.1. Principal Component Analysis

[31] Principal component analysis is analogous to finding the variance from the best fit line (determined by a linear orthogonal regression), where the differences used to calculate the variance are perpendicular to this best fit line. PCA determines the axes of minimum and maximum variability. For unbiased data spanning a much larger range than the uncertainty and for similar small uncertainties in ship and satellite winds, the axis of maximum variability will be very close to the ideal fit. Large difference in these axes would contradict the assumption of similar uncertainties for each data set. For the QSCAT-1 and research vessel comparisons, the angle between axis of maximum variability and the ideal fit line is only 3° for wind directions and 6° for wind speed.

[32] The steps involved in PCA [*Preisendorfer and Mobley*, 1988] are outlined below. The observations are combined into a single matrix **D**.

$$\mathbf{D} = [x_i - \bar{x}, y_i - \bar{y}], \tag{5}$$

where x is one set of observations (e.g., in situ winds), y is the other set (e.g., QuikSCAT winds), and i is an index for the N co-located pairs of winds. The covariance matrix (**C**) can be calculated from **D**.

$$\mathbf{C} = \frac{\mathbf{D}^{\mathrm{T}}\mathbf{D}}{N} = \begin{bmatrix} \sigma_x^2 & \sigma_{xy}^2 \\ \sigma_{xy}^2 & \sigma_y^2 \end{bmatrix} \tag{6}$$

[33] The eigenvalues of **C** are positive and easily obtainable. The larger eigenvalue (λ_1) corresponds to the variance parallel to the axis of maximum variance, and the smaller eigenvalue (λ_2) corresponds to the variance perpendicular to this axis. The uncertainty in the scatterometer observations (corresponding to one standard deviation), for correctly selected ambiguities, is given by the positive square root of λ_2. Owing to our assumptions, this uncertainty is equal to the uncertainty in the research vessel observations. The

Table 5. PCA Derived Uncertainties in SeaWinds Winds Speed (m s^{-1}) and Direction (°) for Various Model Functions and Rain Flags[a]

	MUDH Rain Flag		ENOF Rain Flag		Radiom. Rain Flag	
QSCAT-1	Select Ambiguity	Correct Ambiguity	Select Ambiguity	Correct Ambiguity	Select Ambiguity	Correct Ambiguity
Wind speed	0.82	0.77	0.81	0.76	0.81	0.76
Wind direct.	...	10.8	...	10.6	...	9.7
Zonal wind	1.14	1.02	1.49	1.06	1.60	1.18
Meridional wind	1.13	1.02	1.63	1.03	1.63	0.96
Ku-2000	Ku2000 Flags	Ku2000 Flags			Radiom. Rain Flag	Radiom. Rain Flag
Wind speed	0.65	0.63			0.72	0.70
Wind direct.	...	9.9			...	9.5
Zonal wind	1.87	1.21			1.73	1.15
Meridional wind	2.27	1.33			2.35	1.29

[a]The spatial co-location criterion is differences $\leq$12.5 km.

fraction of variance explained (r^2) can also easily be determined:

$$r^2 = \lambda_2/(\lambda_1 + \lambda_2). \quad (7)$$

These fractions (Table 4) demonstrate the effectiveness of the SeaWinds scatterometer. When averaged over the entire set of co-located data (for correctly selected ambiguities), both model functions account for ~90% of the observed variance in speed and 97% in direction.

[34] PCA can easily be used to investigate the dependency of uncertainties on variables such as wind speed or direction (Figure 7c). This is accomplished by rotating the coordinate system so that the axes of the new system are the axes of maximum and minimum variance. The original axes are rotated by either

$$\theta = 0.5 \text{ atan}\left(\frac{\sigma_{xy}^2}{\sigma_{yy}^2 - \sigma_{xx}^2}\right), \quad (8)$$

or 90° plus this angle (an additional test determines which of these angle corresponds to the axis of maximum variability). The wind directions are rotated to the new axes:

$$x_i' = x_i \cos(\theta) - y_i \sin(\theta) \quad (9)$$

$$y_i' = x_i \sin(\theta) + y_i \cos(\theta) \quad (10)$$

where (x_i', y_i') are the points in the new coordinate system. If j is the index (i) for all values of x within the specified range ($x_1 < x < x_2$), then

$$\sigma_{x,x_1<x<x_2} = \left[\left(\sum_j \left(x_j' - \overline{x'}\right)^2\right)/(n-1)\right]^{0.5}, \quad (11)$$

where $\overline{x'}$ is the mean value for the subset, and n is the number of points in the subset.

[35] For correctly selected ambiguities, wind vectors observed by SeaWinds on QuikSCAT (Table 5) are found to have average uncertainties of ~0.7 m s^{-1} for speed and 10° for direction. The PCA-derived uncertainties show negligible dependence on wind speed. The Ku-2000 GMF uncertainties in wind speed and direction are slightly smaller than the corresponding values from QSCAT-1 GMF. However, the Ku-2000 speed and direction errors are better correlated than the QSCAT-1 errors, resulting in larger errors in zonal and meridional wind components (and non-Gaussian error distributions). A larger majority of well correlated Ku-2000 errors are in the inner swath: the uncertainties for zonal and meridional winds are much smaller for the rest of the swath.

5.2. Vector Correlations

[36] Vector correlations can also be used to assess the relative accuracy of winds [*Freilich*, 1997]. Most techniques for calculating linear correlations suffer from limitation that errors in both sets of observations contribute to a reduction in the magnitude of the correlation. If the uncertainty in the comparison data set is negligible (and there is no bias or gain in these observations), then these correlations can be a useful standard of comparison. However, in the case of open-ocean surface winds, the uncertainty in the comparison data set is not negligible. We will demonstrate a technique that is easily applied and takes advantage of PCA to better account for uncertainty in the truth.

[37] The wind vectors are written as complex numbers (u + iv), with the real component equal to the zonal wind (u), and the imaginary component equal to the meridional wind (v). PCA has been applied to vectors in this form [*Hardy*, 1977; *Hardy and Walton*, 1978; *Legler*, 1983; *Denbo and Allen*, 1984]. These studies examined covariance rather than correlation. Vector correlation can be examined by placing complex wind vectors for in situ and satellite winds in a matrix similar to **D** (equation (5)). The covariance matrix is similar to equation (6):

$$\mathbf{C} = \frac{\mathbf{D}^{\mathrm{T}}\mathbf{D}^*}{N} = \begin{bmatrix} \sigma_x^2 & \sigma_{xy}^2 \\ \sigma_{xy}^2 & \sigma_y^2 \end{bmatrix}, \quad (12)$$

where the star indicates a complex conjugate, and the diagonal terms are the sums of the variance in each component. The diagonal terms represent the sums of u and v variability in each of the data sets.

[38] Principal component analysis is again used to find the axes associated with the minimum and maximum variances. The fraction of variance explained (r^2) is again calculated with equation (7). The magnitude of the correlation $|r|$ (ranging from −1 to 1) can be determined from r^2; however, the sign of r must be determined through visual inspection. In this case, the r^2 values for individual ships are 0.95–0.997 with correctly selected ambiguities and 0.94–0.993 with all selected ambiguities.

5.3. Influence of Spatial Separation Between Co-Locations

[39] Several of the RMS differences for individual ships are substantially lower than the values for other ships. The early R/V *Atlantis* observations (not shown) are an extreme example of low uncertainties: an RMS difference of 0.5 m s^{-1}. An examination of the spatial differences in co-location revealed that most of the R/V *Atlantis* observations were <5 km from the center of QuikSCAT cells, suggesting that this distance could have considerable influence on the estimates of uncertainty. Bilinear interpolation of the QuikSCAT winds to the location of the ship tested the possibility that such dependence was due to linear changes in wind vectors. The impact of such interpolation was small and often slightly unfavorable. This result implies that there is considerable natural variability on spatial scales <25 km, and that if the variability is wavelike then the wavelength varies throughout the co-located data. The sampling volume for the research vessel observations (integrated over space and time) is much smaller than the sampling volume for the scatterometer; consequently, the ship observations are more sensitive to this variability than the scatterometer. However, the weighting within 25 × 5 km scatterometer cells (and within individual footprints) is substantially nonuniform. Therefore, the scatterometer is also sensitive to variability on scales less than the size of the scatterometer's wind cell.

[40] The spatial weighting within the 25 × 25 km wind vector cells is dependent on the distribution of the individ-

ual footprints that are combined to determine a cell's vector wind. In the cases of the current routine products, all 25 × 35 km oval footprints that have centers within the cell are used (with equal weighting) to determine the cell's vector wind (Figure 2). The average weighting distribution within a wind cell can be estimated by assuming a tight (relative to cell size) and uniform distribution of footprints. The number of applicable footprints (those used in calculating the vector wind for the cell) overlapping the center of the cell is more than twice the number at the center of a cell edge, and roughly four times the number at the cell corner. Consequently, the winds near the center of the cell are weighted more heavily than those near the corners and edges. This geometry allows for sensitivity to variability on scales smaller than the cell size.

[41] This hypothesis was confirmed in an examination of σ_w^2 and σ_θ^2 binned as functions of spatial separation between the in situ observations and the center of the scatterometer cell (Figure 8). The range of separations is from 0 to 12.5 km to ensure that all observations are within the closest cell, and to avoid atypically large spatial differences in co-location at the swath edges and near areas of missing data. The variance (σ^2) is examined rather than the standard deviation (i.e., uncertainty, σ) because independent random uncertainties are additive in terms of σ^2 rather than σ. The variance in wind speed (σ_w^2; Figure 8a) for the JPL product has only a small dependence on spatial difference in co-location; however, the Ku-2000 product shows a stronger dependence. The values in the 2.5–5.0 km bins correspond to $\sigma_w = \sim 0.6$ m s^{-1} (similar to the NSCAT random component error) [*Freilich*, 1997; *Freilich and Vanhoff*, 2002]. However, the values in the closest bin are much smaller (corresponding to 0.05–0.3 m s^{-1}). The Ku-2000 products show the clearest trends of reduced uncertainty with reduced difference in co-location. The sensitivity to differences in co-location is expected to greatly decrease for distances less than the half the 5km length scale for the sampling volume of the research ships (i.e., half the smaller of the two sampling volumes). A parabolic curve is likely to best represent the dependence on spatial separation. The data set is too noisy to determine this curve; therefore, we make a conservative estimate by linear extrapolation to 2.0 km. For the radiometer rain flag, the corresponding uncertainty in wind speed is estimated at ~0.45 m s^{-1} for QSCAT-1, and 0.3 m s^{-1} for Ku-2000.

[42] The impact of spatial differences in co-location on direction (Figure 8b), is also large. The appropriate shape for a best fit curve is not clear from these results. A PCA-based parabolic fit to QSCAT-1 RMS differences indicates an uncertainty of ~4°. A more conservative estimate, based on the 0 to 2.5 km bin, indicates $\sigma_\theta = 5°$. The Ku-2000 directional differences are substantially smaller than the QSCAT-1 differences except in the 5 to 7.5 km bin, where they peak. The 0 to 2.5 km bin, and the substantially smaller variances, indicate that the Ku-2000 uncertainty is ~3°. Restricting the Ku-2000 co-locations to the middle (higher quality) part of the swath (not shown) indicates that the directional uncertainty for this part of the swath is ~2°. These results demonstrate the exceptional accuracy of SeaWinds on QuikSCAT and research vessel vector winds, as well as the importance of considering differences in spatial co-locations in any validation effort.

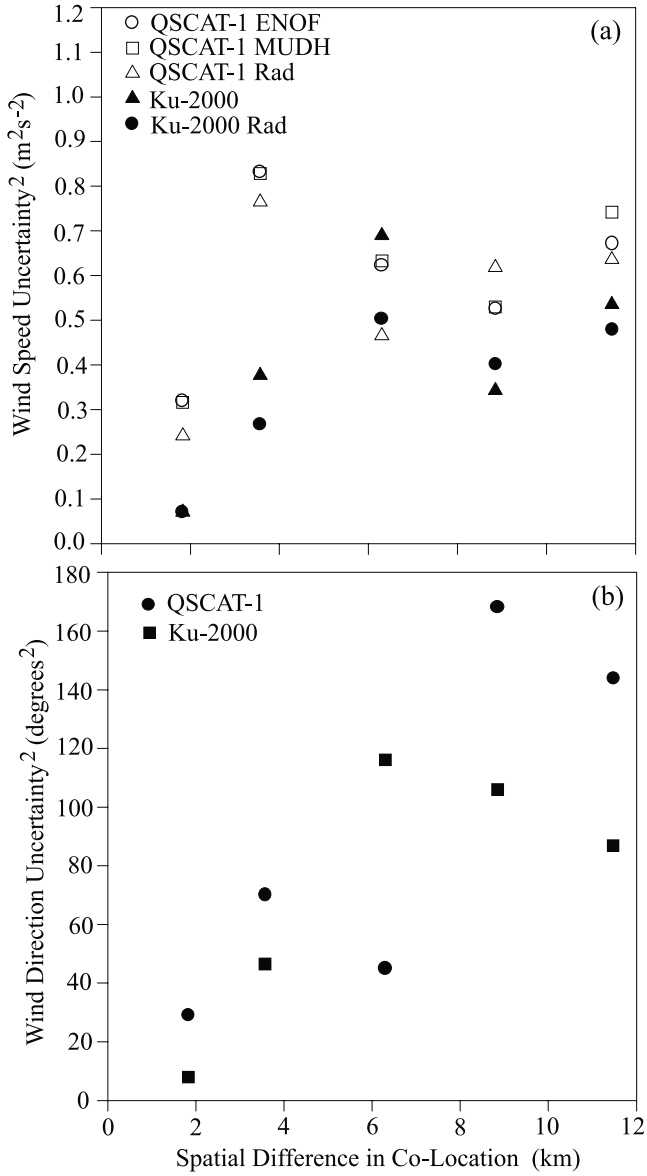

Figure 8. PCA-derived (a) σ_w^2 and (b) σ_θ^2 binned as functions of spatial separation. Bins are in 2.5 km intervals, ranging from 0 to 12.5 km.

[43] The model for uncertainty including spatial variability (σ_s^2) becomes

$$\sigma^2_{|\mathbf{w}|} = \sigma_w^2 + w^2\ \sigma_\theta^2 + \sigma_s^2(\Delta x, w), \tag{13}$$

where σ_s^2 is a function of the spatial difference in co-location (Δx) and wind speed. This term also implicitly considers small-scale variability in the sampling volume and differences between the two sampling volumes. It does not contribute to observational uncertainty. The variability due to spatial co-location differences can be parameterized in terms of contributions due to uncertainties in wind speed (σ_{ws}) and direction ($\sigma_{\theta s}$), both of which are functions of the spatial difference in co-location:

$$\sigma_s^2(\Delta x, w) = \sigma_{ws}^2(\Delta x) + w^2\ \sigma_{\theta s}^2(\Delta x). \tag{14}$$

The values of σ^2_{ws} and $\sigma^2_{\theta s}$ can be estimated from Figures 8a and 8b: for Δx = 6 km, $\sigma^2_{ws} \approx 0.15$ m^2 s^{-2} and $\sigma^2_{\theta s}$ = 40 degrees^2; and for Δx = 8.8 km (the average difference in co-location for data sets limited to 12.5 km), $\sigma^2_{ws} \approx 0.20$ m^2 s^{-2} and $\sigma^2_{\theta s}$ = 75 degrees^2. For both examples, the contribution to directional uncertainty is larger than the corresponding value for SeaWinds observational uncertainty. For comparison of in situ and scatterometer winds, the number of co-locations will be very small for $\Delta x < 6$ km. Consequently, the contribution to total uncertainty from often will be large in comparisons to in situ observations: it must be considered to avoid significant overestimations of observational uncertainty. The influence of temporal difference in co-location is not examined herein, but is also expected to be significant for differences greater than ~3 min (half the maximum time over which scatterometer observations are taken within a cell).

5.4. Contributions to Total Uncertainty

[44] Knowledge of how various problems contribute to the total uncertainty is useful in evaluating where improvements in processing the satellite observations can lead to the greatest reduction in uncertainty. Independent random uncertainties are additive in a RMS sense (i.e., variances are additive). The uncertainty related to direction (for correctly selected ambiguities) is greater than the contribution related to wind speed for $w > 8$ m s^{-1} for the QSCAT-1 GMF, and $w > 18$ m s^{-1} for the Ku-2000 GMF. However, for $w < 8$ m s^{-1} errors in ambiguity become significant. Gross errors in ambiguity selection result in wind vector errors with systematic (directions opposite the true wind vector) and random components. For the purpose of examining contributions to RMS differences, we approximate this component of uncertainty as an entirely random uncertainty in direction ($\sigma_{\theta,a}$). This is not an entirely valid approximation: ambiguity errors have a substantial systematic component in a wind vector relative coordinate system. Furthermore, we ignore ambiguity-related uncertainty in direction ($\sigma_{w,a}$). Future studies should explore these considerations. Herein, ambiguity errors are modeled as an additional source of directional uncertainty, and can be included in equation (14) to model the total observational uncertainty:

$$\sigma^2_{|\mathbf{w}|} = \sigma^2_w + \sigma^2_{w,a} + w^2\left(\sigma^2_\theta + \sigma^2_{\theta,a}\right) + \sigma^2_s(\Delta x, w). \qquad (15)$$

[45] We have few points with which to estimate the dependence of $\sigma_{\theta,a}$ on w, and they are sufficient for only a crude model of uncertainty related to ambiguity selection. Better models for ambiguity-related errors must be developed from other data sets with a much larger number of co-locations. These few points suggest QSCAT-1 and Ku-2000 $\sigma_{\theta,a} = \sim 55°$ at $w = 0$, and $\sigma_{\theta,a} = \sim 0$ at $w = 8$, then QSCAT-1 $\sigma_{\theta,a}$ rises again for greater wind speeds. We empirically approximate the wind speed dependence of $\sigma_{\theta,a}$ for $w < 8$ m s^{-1} as

$$\sigma_{\theta,a} = 55\cos(0.21w), \text{ for } w < 7.5\text{m s}^{-1}. \qquad (16)$$

The cosine function was chosen because of it's slow initial decrease, with a very rapid decrease near the upper limit in wind speed. The function provided to be a much better fit to the very limited data than linear or quadrate functions. However, these results, which are based only on variance due to gross errors in ambiguity, underestimate the uncertainty related to ambiguity selection. This term peaks near w = 4 m s^{-1}, falls rapidly, and is negligible for w = 7.5 m s^{-1}.

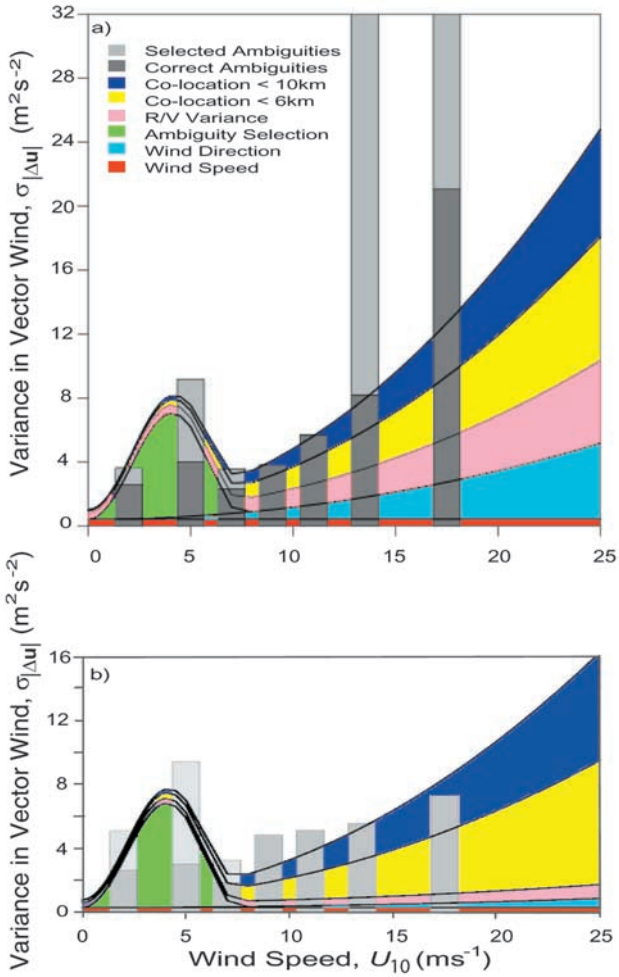

Figure 9. Cumulative contributions to the variance (uncertainty squared) in the magnitude of the vector difference ($\sigma^2_{|\Delta \mathbf{u}|}$) as a function of wind speed for the (a) QSCAT-1 GMF and (b) Ku-2000 GMF. The histograms show the observed values of ($\sigma^2_{|\Delta \mathbf{u}|}$) for correctly selected ambiguities (dark shading) and all selected ambiguities (light plus dark shading). The colored regions show the cumulative variance due to all sources of modeled variance. The order in which these variances are stacked is wind speed (σ^2_g; red), wind direction ($w^2\sigma^2_\theta$; light blue), ambiguity selection ($w^2\sigma^2_{\theta a}$; green), ship observational uncertainty (pink), and spatial differences in co-location (σ^2_g). The yellow shows σ^2_g for a difference in co-location of 6 km, and the total of yellow and blue is for a difference in co-location of 10 km. The uncertainty (1 standard deviation) is equal to the square root of the variance. SeaWinds' observational uncertainty squared is given by the sum of red, light blue, and green variances.

[46] The various contributions to $\sigma^2_{|\mathbf{w}|}$ in equation (15) can be examined (for each GMF) as a function of wind speed (Figure 9) to determine for what conditions reductions in

these uncertainties would have the greatest impact. Variability in $|\Delta\mathbf{u}|$ related to spatial co-location (σ_g) dominates for most wind speeds. Reduction to 20 km cells can reduce variability within cells, and it has been shown to be effective (W.-Y. Tsai, personal communication, 1999); however, reduction below this limit requires smaller footprints or more computationally intensive processing. Of the observational terms (uncertainty in speed (σ_w), uncertainty related to direction ($w\sigma_\theta$), and uncertainty related to ambiguity selection ($w\sigma_\theta$)), for the QSCAT-1 model function, uncertainty related to ambiguity selection dominates for $2.5 < w < 5.5$ m s^{-1}, uncertainty in speed dominates for $w < 2.5$ m s^{-1} and $5.5 < w < 7.5$ m s^{-1}, and uncertainty in direction dominates for $w > 7.5$ m s^{-1}. For the Ku-2000 model function, uncertainty related to ambiguity selection dominates for $0.6 < w < 5.5$ m s^{-1}, uncertainty in speed dominates for $w < 0.6$ m s^{-1} and $5.5 < w < 18$ m s^{-1}, and uncertainty related to direction dominates for $w > 18$ m s^{-1}.

[47] For wind speeds below ~2 m s^{-1}, modified by water temperature [*Pierson et al.*, 1997], atmospheric stratification [*Bourassa et al.*, 1999a], and swell [*Bourassa et al.*, 1999a], there is a wind speed threshold (capillary cutoff) below which short water waves do not exist. Typically, these smooth patches are associated with convective cells with horizontal scales much smaller than the size of the scatterometer footprint. The scatterometer signal is confused due to inhomogeneous wind direction and surface roughness characteristics of the surface: the scatterometer direction should correspond to an average direction within the footprint. In the relatively rare cases where the surface is smooth within the entire footprint, wind directions cannot be found because the radar signal does not interact with short water waves. Therefore, wind directions (and ambiguity selection) below this threshold are random and cannot be improved. Fortunately, the impacts of such errors in meteorological and oceanographic applications are likely to be negligible. For $w < 5.5$ m s^{-1} (i.e., approximately half of ocean winds), improvements in ambiguity selection are likely to have the greatest impact in reducing errors in scatterometer winds.

[48] It should be emphasized that these results are across−swath averages. The accuracy in the middle swath is superior to these results, and the accuracy in the inner swath (near nadir) and the outer swath (near the edges) is considerably worse. Improving accuracy in these regions could have a relatively strong impact on the average accuracy.

[49] The model for uncertainty (equation (15)) can be verified through comparisons of modeled RMS of the magnitude of differences ($|\Delta\mathbf{w}|_{\mathrm{rms}}$) to observed values of $|\Delta\mathbf{w}|_{\mathrm{rms}}$. The modeled value of $|\Delta\mathbf{w}|^2_{\mathrm{rms}}$ is equal to the uncertainty squared in equation (15) plus the uncertainty squared of the ship's observations (ship uncertainty is assumed to be equal to the scatterometer's uncertainty for correctly selected ambiguities).

$$|\Delta\mathbf{w}|^2_{\mathrm{rms}} = \sigma^2_{w,\mathrm{scat}} + \sigma^2_{w,\mathrm{ship}} + w^2\left(\sigma^2_{\theta,\mathrm{scat}} + \sigma^2_{\theta a} + \sigma^2_{\theta,\mathrm{ship}}\right) + \sigma^2_g(\Delta x, w) \tag{17}$$

[50] These RMS differences are shown (Figure 9) for both the QSCAT-1 and Ku-2000 GMFs. The error model (dash-dotted line) is a good match to $|\Delta\mathbf{w}|^2_{\mathrm{rms}}$, except for the QSCAT-1 problems ambiguity selection for $w > 8$ m s^{-1} which are not captured (it was not considered in the model). The peak in ambiguity selection related uncertainty (at $w = 4$ m s^{-1}) is also underestimated due to our consideration of only gross ambiguity selection errors. Replacing the variance for low wind speeds in equation (16) with a value of 65° results in much better matches (not shown).

[51] This study has demonstrated that there is substantial variability in speed and direction on length scales smaller than the scatterometer cell size (25 km). This variability contributes to what is perceived as noise in the backscatter, and hence it causes additional uncertainty in determining both speed and direction. This study suggests a preliminary physical basis from which the signal-to-noise ratio can be optimized in terms of cell size and footprint size.

6. Summary

[52] Accuracy of rain-free vector winds is assessed through two techniques. One technique is a new PCA-based method for determining vector correlations. The fraction of variance explained by assuming a linear relationship between in situ and satellite wind vectors was between ~90% and 99.7% for correctly selected ambiguities and only slightly smaller for all selected ambiguities. Wind vector uncertainty was also defined through the standard deviation in the magnitude of vector errors ($|\mathbf{w}_{\mathrm{scat}} - \mathbf{w}_{\mathrm{ship}}|$). An error model (equation (17); Figure 9) based on the above results accounts for five contributions to uncertainties as functions of wind speed. It also considers differences in satellite and in situ winds due to differences in spatial co-locations, which implicitly considers differences in sampling volume. The function for observational uncertainty can be used in conjunction with the variability as a function of spatial difference in co-location (Figure 8) to provide a preliminary basis from which the scatterometer's signal-to-noise ratio can be optimized in terms of cell size and footprint size. A reduction in footprint size would reduce the spatial variability within cells. If this reduction in size does not result in too great a loss of signal, it would increase the accuracy of scatterometer wind speed and direction as well as the fine spatial scales of fronts and small-scale circulations.

[53] Estimates of uncertainty in an instrument must consider the accuracy of the data used as the standard of comparison. There is no absolute standard for wind speed and direction measurements over the open ocean. The uncertainty in our comparison measurements is unknown and varies from ship to ship and cruise to cruise. Principal component analysis (PCA) is an excellent tool for error analysis when the uncertainty is similar in the test data set and the comparison measurements. This assumption of similarity is valid if the uncertainties in both data sets are small compared to the span of the observations, as they are in this case.

[54] We demonstrate that differences in spatial co-location have significant impact on RMS differences (Figure 9), and that these differences can dominate instrument dependent sources of uncertainty of $w > 4.5$ m s^{-1} when spatial co-location is within 10.0 km. The observational uncertainty in the instrument can be estimated by plotting uncertainty as a function of co-location distance and then extrapolating the observed uncertainties to an exact spatial co-location. This procedure results in conservative estimates of QSCAT-1

(Ku-2000) uncertainties, for rain-free conditions, of 5° (3°) for direction and 0.45 m s^{-1} (0.3 m s^{-1}) for speed. This assessment of directional accuracy does not consider errors in ambiguity selection, which peak near $w = 4$ m s^{-1}, dominates instrument and GMF related uncertainty for $w <$ 5.5 m s^{-1}, and has some across-swath dependence. The QSCAT-1 model function also has ambiguity selection errors in the inner swath (near nadir) for $w > 12$ m s^{-1}, which contribute to very large vector differences.

[55] **Acknowledgments.** The QSCAT-1 scatterometer data were obtained from the NASA Physical Oceanography Distributed Active Archive Center at the Jet Propulsion Laboratory/California Institute of Technology, and the Ku-2000 scatterometer data was provided by Frank Wentz and Deborah Smith at Remote Sensing Systems. Research vessel observations were provided by Barrie Walden (WHOI; R/V *Atlantis* and R/V *Oceanus*), Mark Rosenberg (Antarctic Cooperative Research Center; RSV *AuroraAustralis*), Woody Sutherland (SIO; R/V *Melville*), Volker Wagner (Marine Data Service, Deutscher Wetterdienst Geschdftsfeld Seeschiffahrt; R/V *Meteor*), Gert Koenig-Langlo (Alfred Wegener Institute for Polar and Marine Research; R/V *Polarstern*), and Dennis Shields and Jonathan Shannahoff (NOAA Corps Operations; R/V *Ronald Brown*). We thank Mike H. Freilich (Oregon State University) for his many helpful comments and insights. Support for the scatterometer research came from the NASA/OSU SeaWinds project and the NASA OVWST project. NSF support of the WOCE DAC/SAC for surface meteorology funded quality control of research vessel data. COAPS receives base funding from the Secretary of Navy Grant from ONR to James J. O'Brien.

References

Atlas, R., S. C. Bloom, R. N. Hoffman, E. Brin, J. Ardizzone, J. Terry, T. D. Bungato, and J. C. Jusem, Geophysical validation of NSCAT winds using atmospheric data and analyses, *J. Geophys. Res.*, *104*, 11,405–11,424, 1999.

Bliven, L. F., H. Branger, P. W. Sobieski, and J.-P. Giovanageli, An analysis of scatterometer returns from a water surface agitated by artificial rain, *Int. J. Remote Sens.*, *14*, 2315–2329, 1993.

Bourassa, M. A., M. H. Freilich, D. M. Legler, W. T. Liu, and J. J. O'Brien, Wind observation from new satellite and research vessels agree, *Eos Trans. AGU*, *78*, 597–602, 1997.

Bourassa, M. A., D. G. Vincent, and W. L. Wood, A flux parameterization including the effects of capillary waves and sea state, *J. Atmos. Sci.*, *56*, 1123–1139, 1999a.

Bourassa, M. A., L. Zamudio, and J. J. O'Brien, Noninertial flow in NSCAT observations of Tehuantepec winds, *J. Geophys. Res.*, *104*, 11,311–11,320, 1999b.

Caruso, M. J., S. Dickinson, K. A. Kelly, M. Spillane, L. J. Mangum, M. McPhaden, and L. D. Stratton, Evaluation of scatterometer winds using equatorial Pacific buoy observations, *WHOI-99-10*, Woods Hole Oceanogr. Inst., Woods Hole, Mass., 1999.

Chelton, D. B., M. H. Freilich, and S. K. Esbensen, Satellite observations of the wind jets off Central America, part I, Case studies and statistical characteristics, *Mon. Weather Rev.*, *128*, 1993–2018, 2000a.

Chelton, D. B., M. H. Freilich, and S. K. Esbensen, Satellite observations of the wind jets off Central America, part II, Regional relationships and dynamical considerations, *Mon. Weather Rev.*, *128*, 2019–2043, 2000b.

Cornillon, P., and K.-A. Park, Warm core ring velocity inferred from NSCAT, *Geophys. Res. Lett*, *28*, 575–578, 2001.

Denbo, D. W., and J. S. Allen, Rotary empirical orthogonal function-analysis of currents near the Oregon coast, *J. Phys. Oceanogr.*, *14*, 35–46, 1984.

Foster, R. C., R. A. Brown, and A. Enloe, Baroclinic modification of mid-latitude marine surface wind vectors observed by the NASA scatterometer, *J. Geophys. Res.*, *104*, 31,225–31,237, 1999.

Freilich, M. H., Validation of vector magnitude datasets: Effects of random component errors, *J. Atmos. Oceanic Technol.*, *14*, 695–703, 1997.

Freilich, M. H., and R. S. Dunbar, The accuracy of the NSCAT 1 vector winds: comparisons with National Data Buoy Center buoys, *J. Geophys. Res.*, *104*, 11,231–11,246, 1999.

Freilich, M. H., and B. A. Vanhoff, The accuracy of remotely sensed surface wind speed measurements, *J. Atmos. Oceanic Technol*, in press, 2002.

Gonzales, A. E., and D. G. Long, An assessment of NSCAT ambiguity removal, *J. Geophys. Res.*, *104*, 11,449–11,458, 1999.

Graber, H. C., A. Bentamy, and N. Ebuchi, Evaluation of scatterometer winds with ocean buoy observations, paper presented at NASA Scatterometer Symposium, Scatterometer Proj. Off., Jet Propul. Lab., Maui, Hawaii, 1997.

Hardy, D. M., Empirical eigenvector analysis of vector observations, *Geophys. Rev. Lett.*, *4*, 319–320, 1977.

Hardy, D. M., and J. J. Walton, Principal components analysis of vector wind measurements, *J. Appl. Meteorol.*, *17*, 1153–1162, 1978.

Huddleston, J. N., and B. W. Stiles, A multidimensional histogram rain-flagging technique for SeaWinds on QuikSCAT, paper presented at IEEE Geoscience and Remote Sensing Symposium, Inst. of Elctr. and Electr. Eng., Honolulu, Hawaii, 2000.

Kelly, K. A., S. Dickinson, M. J. McPhaden, and G. C. Johnson, Ocean currents evident in satellite wind data, *Geophys. Res. Lett.*, *28*, 2469–2472, 2001.

Kent, E. C., P. K. Taylor, and P. Challenor, A comparison of ship and scatterometer-derived wind speed data in open ocean and coastal areas, *Int. J. Remote Sens.*, *19*, 3361–3381, 1998.

Large, W. G., J. Morzel, and G. B. Crawford, Accounting for surface wave distortion of the marine wind profile in low-level ocean storms wind measurements, *J. Phys. Oceanogr.*, *25*, 2959–2971, 1995.

Legler, D. M., Empirical orthogonal function analysis of wind vectors over the tropical Pacific region, *Bull. Am. Meteorol. Soc.*, *64*, 234–241, 1983.

Liu, W. T., and W. Tang, Objective interpolation of scatterometer winds, *Tech. Rep. 96-19*, Jet Propul. Lab., Calif. Inst. of Technol., 1996.

Mears, C., D. Smith, and F. Wentz, Detecting rain with QuikSCAT, paper presented at International Geoscience and Remote Sensing Symposium, Inst. of Electr. and Electr. Eng., Honolulu, Hawaii, 2000.

Mears, C., D. Smith, and F. Wentz, Comparison of Special Sensor Microwave Imager and buoy-measured wind speeds from 1987 to 1997, *J. Geophys. Res.*, *106*, 11,719–11,729, 2001.

Milliff, R. F., T. J. Hoar, H. van Loon, and M. Rapheal, Quasi-stationary wave variability in NSCAT winds, *J. Geophys. Res.*, *104*, 11,425–11,436, 1999a.

Milliff, R. F., W. G. Large, J. Morzel, G. Danabasoglu, and T. M. Chin, Ocean general circulation model sensitivity to forcing from scatterometer winds, *J. Geophys. Res.*, *104*, 11,337–11,358, 1999b.

Moore, R. K., D. Chatterjee, and S. Taherion, Algorithm for correcting SeaWinds/ADEOS-II for rain attenuation, paper presented at QuikSCAT Cal/Cal-Early Science Meeting, Scatterometry Proj. Off., Jet Propul. Lab., Arcadia, Calif., 1999.

Naderi, F. M., M. H. Freilich, and D. G. Long, Spaceborne radar measurements of wind velocity over the ocean—An overview of the NSCAT scatterometer system, *Proc. of the IEEE*, *79*, 850–866, 1991.

Pearson, K., On lines and planes of closest fit to systems of points in space, *Philos. Mag.*, *2*, 559–572, 1901.

Pierson, W. J., Jr., Examples of, reasons for and consequences of the poor quality of wind data from ships for the marine boundary layer: Implications for remote sensing, *J. Geophys. Res.*, *95*, 13,313–13,340, 1990.

Pierson, W. J., Jr., M. A. Donelan, D. G. Long, and W. B. Sylvester, The measurement of calms, light air and light to moderate breezes by NSCAT, paper presented at NASA Scatterometer Symposium, Scatterometer Proj. Off., Jet Propul. Lab., Maui, Hawaii, 1997.

Preisendorfer, R. W., and C. D. Mobley, Algebraic foundations of PCA, in *Principal Component Analysis in Meteorology and Oceanography*, pp. 11–24, Elsevier Sci., New York, 1988.

Shaffer, S. J., R. S. Dunbar, S. V. Hsaio, and D. G. Long, A median-filter-based ambiguity removal algorithm for NSCAT, *IEEE Trans. Geosci. Remote Sens.*, *29*, 167–174, 1991.

Smith, S. R., C. Harvey, and D. M. Legler, Handbook of quality control procedures and methods for surface meteorology data, *WOCE Rep.141/96*, 56 pp., World Ocean Circ. Exp., Data Assem. Cent., Cent. Ocean-Atmos. Predict. Stud., Fla. State Univ., Tallahassee, Florida, 1996.

Smith, S. R., M. A. Bourassa, and R. J. Sharp, Establishing more truth in true winds, *J. Atmos. Oceanic Technol.*, *16*, 939–952, 1999.

Sobieski, P. W., and L. F. Bliven, Analysis of high speed images of raindrop splash products and Ku-band scatterometer returns, *Int. J. Remote Sens.*, *16*, 2721–2726, 1995.

Sobieski, P. W., C. Craeye, and L. F. Bliven, Scatterometric signatures of multivariate drop impacts on fresh and salt water surfaces, *Int. J. Remote Sens.*, *20*, 2149–2166, 1999.

Stoffelen, A., Toward the true near-surface wind speed: Error modeling and calibration using triple co-location, *J. Geophys. Res.*, *103*, 7755–7766, 1998.

Taylor, G. I., The spectrum of turbulence, *Proc. R. Soc. London, Ser. A*, *67*, 16–20, 1938.

Taylor, P. K., E. C. Kent,M. J. Yelland, and B. I. Moat, The accuracy of marine surface winds from ships and buoys, papers presented at WMO Workshop on Advances in Marine Climatology—CLIMAR99, World Meteorol. Org., Vancouver, Can., 1999.

Thiebaux, M. L., Wind tunnel experiments to determine correction functions for shipborne anemometers, *Can. Contract. Rep. Hydrog. Ocean*

Sci. 36, 57 pp., Bedford Inst. of Oceanogr., Dartmouth, Nova Scotia, 1990.

Verschell, M. A., M. A. Bourassa, D. E. Weissman, and J. J. O'Brien, Model validation of the NASA Scatterometer winds, *J. Geophys. Res.*, *104*, 11,359–11,374, 1999.

Weissman, D. E., M. A. Bourassa, and J. Tongue, Effects of rain-rate and wind magnitude on SeaWinds scatterometer wind speed errors, *J. Atmos. Oceanic*, *19*, 738–746, 2000.

Wentz, F. J., and D. K. Smith, A model function for the ocean-normalized radar cross section at 14 GHz derived from NSCAT observations, *J. Geophys. Res.*, *104*, 11,499–11,514, 1999.

Yelland, M. J., B. I. Moat, P. K. Taylor, R. W. Pascal, J. Hutchings, and V. C. Cornell, Wind stress measurements from the open ocean corrected for airflow distortion by the ship, *J. Phys. Oceanogr.*, *28*, 1511–1526, 1998.

Zierden, D. F., M. A. Bourassa, and J. J. O'Brien, Cyclone surface pressure fields and frontogenesis from NASA Scatterometer (NSCAT) winds, *J. Geophys. Res.*, *105*, 23,967–23,981, 2000.

M. A. Bourassa, J. J. O'Brien, and S. R. Smith, Center for Ocean-Atmospheric Prediction Studies, Florida State University, Tallahassee, Florida 32306, USA. (bourassa@coaps.fsu.edu)

D. M. Legler, U.S. CLIVAR Office, 400 Virginia Ave. SW, Suite 750, Washington, D.C. 20024, USA.